Sixth International Symposium on Marine Propulsors
smp'19, Rome, Italy, May 26-30, 2019

Thrust Losses and Dynamic Loads on a Ducted Pushing Thruster in Regular Waves

Vladimir Krasilnikov[1], Nabila Berchiche[2] and Kourosh Koushan[1]

[1]SINTEF Ocean, Ships and Ocean Structures, Trondheim, Norway, [2]formerly SINTEF Ocean

ABSTRACT

This paper presents the results of CFD investigations into the hydrodynamics of a ducted azimuth propulsor operating in regular waves. Numerical simulations are conducted to quantify thrust losses and load oscillations experienced by the propulsor in waves of different height and magnitude, without and with the occurrence of ventilation. In addition to the scenarios when propulsor submergence is fixed, wave induced planar motions of propulsor in the roll plane are also studied. The findings highlight the importance of dynamic effects in the flow, which are associated with wave passage and propulsor motion, especially when the ventilation phenomenon is involved.

Keywords

Azimuth propulsor, Regular waves, Planar motions, Ventilation, CFD.

1 INTRODUCTION

Marine operations performed by offshore vessels become increasingly challenging. Harsh and highly changeable weather conditions in exposed sea regions, increased density of traffic near the shore and in harbours, and complexity of maneuvering scenarios set priority on operational safety, in general, and performance of propulsors, in particular. In order to avoid most unfavorable situations, one needs accurate and reliable data regarding thrust losses under different conditions, and dynamic loads on propulsor components. The mechanical failures in gears and bearings of azimuth propulsors installed on offshore vessels are reported to be associated with extreme maneuvers, impact of slipstream from the neighboring propulsor and occurrence of ventilation (Dang, 2013). The ventilation phenomenon may develop during both the low-speed maneuvering (approach to an offshore structure, DP, docking) and free-sailing, and it depends on propulsor submergence and loading. Ventilation is a naturally unsteady phenomenon. The degree of its unsteadiness, and hence the associated load oscillations on propulsor may be amplified significantly by the influence of waves. In such a scenario, the propulsor submergence would vary due to passage of wave crests and troughs as well as due to wave induced vessel motions. Further, the passing waves induce the field of orbital velocities around the propulsor, while propulsor accelerations contribute to even higher gradients of load variation. However, both the experimental studies (Koushan, 2007) and numerical studies (Berchiche et al, 2017) point out at ventilation as the phenomenon responsible for largest load oscillations, as on whole propulsor as on the individual propeller blades.

Dynamic loads on a propeller blade subject to ventilation in behind hull conditions have been investigated by model tests (van Beek and van Terwisga, 2006). Extensive research on ventilation effect on podded propulsors has been performed in (Koushan, 2006a; 2006b; 2007). The latter investigations include the cases of open and ducted pushing pod propulsor and consider the situations with fixed propulsor submergence and sinusoidal heave motion near the free surface. The data are acquired regarding the loads acting on one propeller blade, on the duct (for the ducted arrangement), and integral forces on propulsor. In particular, it is shown in (Koushan, 2006b) that when a ducted propulsor operates at bollard, at fixed submergence of H/Dp=0.5 (where Dp is the propeller diameter, and H is the vertical distance from free surface to propeller shaft axis), the duct loses about 95% of its thrust, while propeller loses about 80% of its thrust. These figures correlate very well with the magnitudes of thrust losses predicted from CFD analyses carried out on the same propulsor in (Berchiche et al, 2017; 2018). It has also been shown by both the experimental measurements (Koushan, 2006b; 2007) and numerical simulations (Berchiche et al, 2017; 2018) that onset of ventilation is associated with a rapid increase of blade loads oscillation, which is noticed at low-speed operation as well as in free-sailing. Further, the numerical analyses conducted in the referred work by the authors reveal different mechanisms of ventilation inception observed at low-speed operation (heavy propeller loading) and in free-sailing (light propeller loading). Under the conditions of light propeller loading, propulsor ventilation develops as a sudden pocket-like deformation of the free surface above the propulsor, at the submergence around H/Dp=0.7. There is no air entrainment by propeller blades, so that the air fraction remains limited to the upper part of propeller disk. In the case of heavy propulsor loading, the mechanism of ventilation inception is associated with the

formation of vortices extending from the free surface, along the propulsor strut, to the suction side of the propeller blade, or to the inner side of the duct near the blade tip. The occurrence of ventilation event is registered at H/Dp=0.8 at bollard (J=0.0), and H/Dp=0.9 at trawling (J=0.2), and it is accompanied by air entrainment by the propeller blades on the duct interior surface.

Since ventilation is identified as a primary cause of strong load fluctuations even at fixed position of propulsor under the free surface, it is obvious that its negative impact on propulsor would be even greater in waves. Experimental studies have been conducted with open pushing and pulling pod propulsors in regular waves in (Koushan et al, 2009; 2011). It is observed that, for all ventilated conditions, a sudden drop of thrust occurs at a certain critical advance coefficient, J, which depends on propeller pitch setting (hence, propeller loading) and submergence. In this sub-critical range, the effect of wave height is significant. Time-variations of propeller thrust and torque follow free surface elevation. Maximum thrust losses are normally registered in the vicinity of wave troughs where maximum amount of ventilation is found. The experiments involving ventilation on open pulling pod propellers in waves have also been conducted in (Deng et al, 2013). The findings from this work show that blade load amplitudes reach their maximum during the passage of wave crests, while the averaged blade thrust is lowest. During trough passage, the load amplitudes are much lower, but the averaged blade thrust increases. These results give indication that propeller blades experience quite different inflow due to the changes in orbital velocities induced by waves. In addition to the above, the occurrence of "extreme" events associated with sudden high peaks of blade load amplitudes is reported. While the origin of these events is not entirely clear, it is hypothesized that they are caused by collapse of large air pockets.

All the aforementioned studied indicate the importance of dynamic phenomena involved in the hydrodynamics of propulsor operating near free surface. A deeper insight into the actual flow mechanisms behind the results can be gained through numerical simulations. CFD analyses such as conducted in (Califano, 2010), (Berchiche et al, 2017; 2018) are still very challenging due to both the complex physics modelling and heavy demand on computational resources. Nevertheless, in the present study, an attempt is made by the authors to extend the earlier developed numerical model to the case of propulsor operation in regular waves and subject to forced planar motions, including heave, sway and roll, as well as the combined motion. The simulations are performed by the unsteady RANS method, using a two-phase (water-air) fluid formulation to investigate the influence of regular waves of different period and height on propulsor characteristics at bollard and free-sailing operation, in open water conditions, i.e. without the presence of ship hull. The forced propulsor motions are so far studied for the conditions of heavy loading (J=0.0 and 0.3). Simulations are performed under the conditions without and with the occurrence of ventilation to understand separate contributions to thrust losses and blade load fluctuations arising from different factors such as wave-induced orbital velocities, propulsor motions and ventilation event.

2 NUMERICAL APPROACH

The numerical approach employed in the present study follows the main principals of the method proposed in (Berchiche at al, 2017; 2018) for the simulation of azimuth propulsor in oblique flow conditions and in presence of initially undisturbed free surface. It solves the unsteady RANS equations within the frameworks of a finite volume method formulation, using a segregated solver. In order to resolve the interaction between the rotating propeller and stationary components of propulsor such as pod and duct, the mesh region surrounding propeller is separated from the outer fluid, and during the solution it participates in rotational motion around propeller shaft axis. The sliding mesh interfaces are applied between the propeller region and outer fluid region. The implicit unsteady solution is performed with a first-order temporal discretization scheme and time step corresponding to 1 degree of propeller rotation. The flow is assumed fully turbulent, and the Shear-Stress-Transport (SST) k-ω model with All Y+ near-wall modelling algorithm is used for turbulence closure. The two-phase fluid is considered using the Eulerian Multiphase Mixture model with the Volume of Fluid (VOF) method. The High-Resolution Interface Capturing (HRIC) scheme is used for tracking the water-air interface. The default settings of the HRIC scheme in STAR-CCM+ are adopted (second-order convection scheme, sharpening factor 0.0, angle factor 0.5, CFL_l=0.5, CFL_u=1.0). No phase interaction and phase change are allowed in the solution, so that cavitation is not modelled in the problems with free surface, even though it would develop in a realistic flow, under simulated conditions. The geometry modeling, meshing and solution are performed with the commercial CFD software STAR-CCM+ (versions 12.02 and 12.04). The results of comprehensive validation studies with this method have been presented in (Berchiche et al, 2017; 2018), including comparisons between the calculations and model tests data in terms of forces and moments acting on all propulsor components and single blade loads.

In the present work, the basic approach described above was significantly revised and extended to accommodate the models for free surface waves and planar motions of propulsor. The following main changes were introduced.

The meshing method was changed to an entirely Parts Based approach instead of Region Based approach. This

approach allows for decoupling physics from meshing, and it offers greater flexibility and automation when handing the geometries.

The size of rectangular computation domain (X×Y×Z) was increased from approximately (44Dp×20Dp×20Dp) in the previous method to (200Dp×200Dp×40Dp) in the new method. A larger domain is needed to accommodate sufficient number of wave lengths in the simulations of propulsor in regular waves, and it is also better suited for calculations in oblique flow conditions.

Prism mesh extrusion towards Inlet and Outlet boundaries is not used any longer. Mesh without extrusion requires more care during mesh generation process, and it is generally more expensive as regards total cell count. However, it is better suited for oblique flow, planar motions and propulsor azimuthing scenarios, especially if an adaptive mesh refinement is eventually applied.

While the solution with two sliding mesh interfaces (upstream and downstream) was used successfully in the previous simulations, in the new approach the decision was made in favour of three sliding interfaces. The third, circumferential sliding interface is added in the gap between the propeller blade tip and duct interior surface. Such a configuration allows to avoid solution contamination that was found to occur in the previous approach, in the areas where the upstream and downstream mesh interfaces intersected the duct surface (in particular, when the mesh in those areas was not very fine).

Both the moving mesh method and overset mesh method are implemented in the present setup. The overset mesh method offers more generalization and a greater flexibility when modeling complex scenarios such as for example simultaneous forced heave motion and azimuthing of propulsor near the free surface, or ship motions in waves with operating propulsors.

In the present work, both the moving mesh method and overset mesh method are implemented to support mesh motion and DFBI motion algorithms to model propulsor motion.

The total cell count in the computation mesh was reduced somewhat compared to the previous case due to a more elaborate system of volumetric controls that apply a finer mesh in the areas where the flow needs to be resolved more accurately, and that use a coarser mesh in the less significant areas. The examples of areas that require especially fine mesh are given by the domains around and downstream of pod and propeller, the blade tip/gap region, and free surface. For the setup without free surface as illustrated in Figure 1, the total cell count is about 12 mil cells, of which 3.4 mil cells are in the propeller region, and 8.6 mil cells are in the region of outer fluid, including the prism cell layers placed along the wall boundaries such as

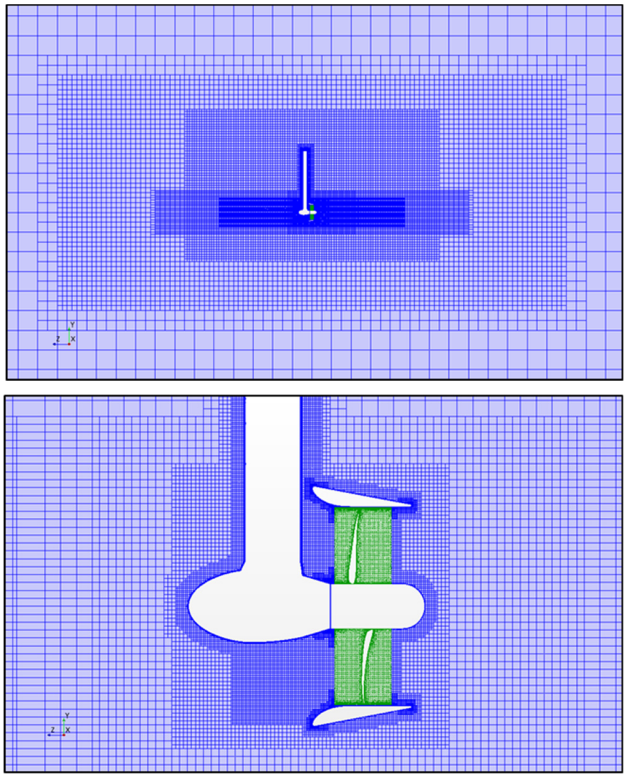

Figure 1: Overall refinement pattern in the computation mesh used in the moving mesh method (setup without free surface).

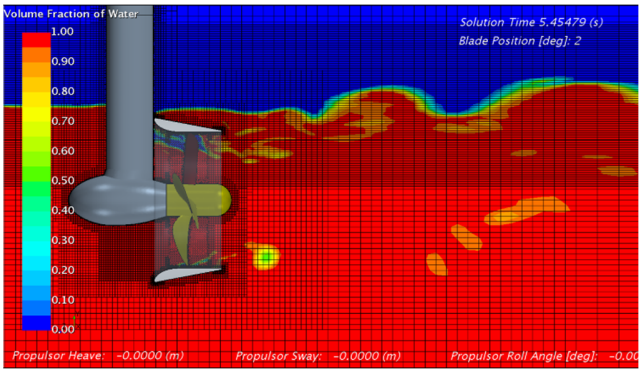

Figure 2: Mesh refinement near free surface in the problem addressing propulsor ventilation.

propeller, duct and pod. For the problems involving free surface, additional mesh refinement is required in the vicinity of free surface. One needs to ensure sufficient extension of the free surface refinement control in the vertical direction and sufficient number of cells in both the vertical and horizontal directions, in order to resolve free surface deformations caused by ventilation event and oncoming waves. In the present setup, the cell size of 1% of propeller diameter, Dp, is applied in Z-direction (vertical),

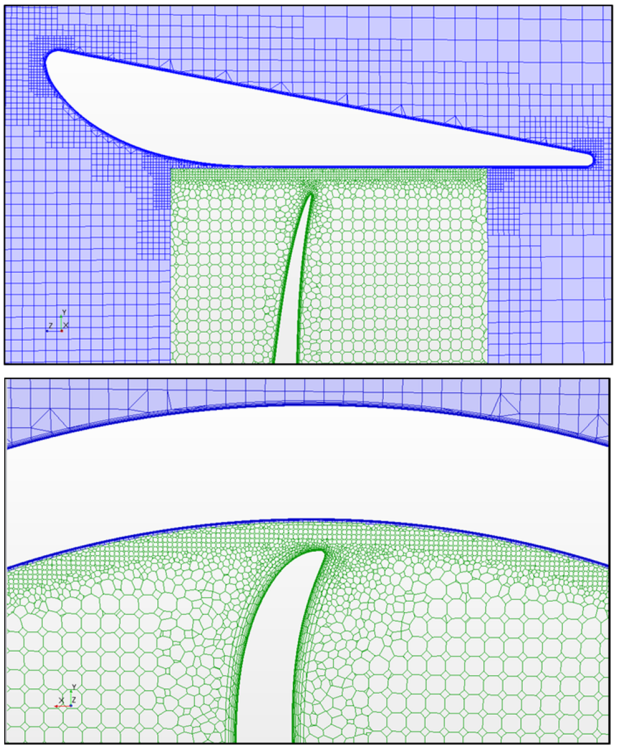

Figure 3: Details of computation mesh in the propeller region and tip clearance area.

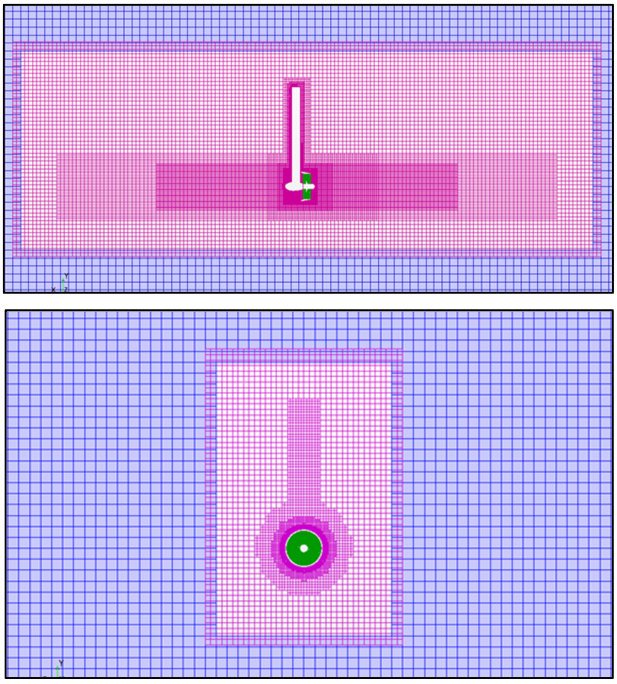

Figure 4: Three mesh regions in the overset mesh method. (blue – outer fluid, background, stationary; magenta – overset, moving as prescribed; green – propeller region, rotating with respect to overset region)

in the free surface volumetric control that extends through the whole domain in X-Y-directions at the water level, for the simulations with initially calm free surface, see Figure 2. In the problems involving regular waves, this value may require adjustment as one needs to control the number of cells per wave height and wave length. In general, 40-50 cells per wave height and 120-160 cells per wave length are recommended for this type of simulations. The resulting free surface mesh is on a finer side compared to general recommendations given in (ITTC, 2011; 2013) for modeling free surface in ship flow problems. This is due to the fact that a higher degree of resolution is required in the case of strong free surface deformations caused by the interaction of waves with propulsor strut piercing the free surface, and by the ventilation event. The desired mesh refinement pattern is achieved by anisotropic refinement in the trimmed hex mesh and by an additional volumetric controls around propulsor. With the above mesh refinement settings, the total cell count reaches 17-18 mil in the problems with initially calm free surface, and 23-25 mil in the problems with regular waves.

The target cell size in the propeller region and the area surrounding the propulsor is set equal to 1% of Dp, while a finer mesh is applied in the areas of tip clearance and duct edges (0.25% of Dp). In the propeller region, the polyhedral mesh is built using the advancing layer meshing method. In the region of outer fluid, the mesh is trimmed, predominantly hexahedral. Figure 3 illustrates some details of the mesh in the propeller region, around the duct, and in the tip clearance area.

The overset mesh is produced following generally the same refinement patterns as the moving mesh. The main difference is that it contains one more region – the overset mesh region, which surrounds the propulsor and moves according to the user prescribed motion model. The overset region is shown by magenta colour in Figure 4. As before, the propeller region is rotating around the propeller shaft axis, and it participates in the motion together with the overset region. The outer fluid region in the overset mesh method is always stationary, whereas in the former, moving mesh method it can be either stationary or moving.

There are different ways to set up the desired motion of propulsor in STAR-CCM+. The forced planar motions can be set up using the general DFBI Rotation and Translation method with the Planar Motion Carriage option. Within this option, the model "General Planar Motion" is available, where one can set up a three-component motion either in the roll plane (heave, sway, roll) or in the pitch plane (heave, surge, pitch), or in the yaw plane (surge, sway, yaw). A sinusoidal oscillatory motion is prescribed according to the following equation:

$$r(t) = Amp \cdot sin(2 \cdot \pi \cdot f \cdot t + \varphi), \qquad (1)$$

where Amp is the motion amplitude, $f = \omega/2\pi = 1/T$ is the motion frequency, φ is the phase angle, T is the period, and t is the time. The motions are defined in the Lab coordinate system. A body-fixed coordinate system "Propulsor-CSys" is introduced, which follows propulsor motions in the DFBI solution. In addition to that, the coordinate system "Thruster-CSys" is introduced as a local coordinate system under "Propulsor-CSys". The X-axis of the "Thruster-CSys" always points forward, in the direction of shaft axis. In this way one can model the situations where propulsor is installed at non-zero heading, heeling and tilting angles. The Lab and "Thruster-CSys" coordinate systems are shown in Figure 5. The rotational motion of propeller region is superposed on the DFBI Rotation and Translation motion, and it is defined with respect to the X-axis of the coordinate system "Thruster-CSys". One of the propeller blades is defined as a separate boundary in the propeller region, and its position is tracked by the current blade angle, which is computed in the "Thruster-CSys". This blade is used for the output of single blade loads.

The alternative to DFBI method is to use the mesh motion method, where the same motions can be set as forced translational and rotational motions through the velocity equations, using motion managed coordinate systems. While the latter method is more general, one inconvenience is related to the fact that pitch and roll motions need to be set up by means of corresponding "rotation rates".

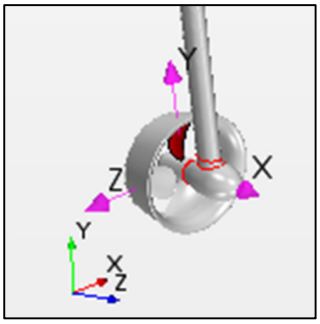

Figure 5: Coordinate systems used in the propulsor motion setup. (coordinate system "Thruster-CSys" is shown by magenta colour; the blade marked by red colour is the key blade for which single blade loads are computed)

For modelling regular waves, the fifth order VOF wave model is employed, where such wave parameters as wave height, wave period, wave velocity and wave direction are specified. The wave velocity and direction can in principal be different from the direction of current and wind, although such situations are not considered in the present study. The waves are assumed to arrive on the propulsor from ahead and their speed equals to the speed of advance of propulsor. The second order discretization scheme is used in the VOF method of STAR-CCM+. The order of discretization scheme is an important parameter that determines the required number of cells per wave length as mentioned above. It has been found during the calculations that simulation with regular waves may develop instabilities and either diverge or yield non-physical results, if the domain outlet is placed too close to propulsor. This is one important reason for using a large computation domain as in the present study. At least 2-3 wave lengths can be recommended as the distance from propulsor location to domain outlet. For shorter domain, wave forcing applied at the outlet may remedy the situation, if solution instabilities occur.

In order to validate the revised numerical setup, a number of test calculations have been carried out. In the first exercise, the case of propulsor operating at J=0.3 in straight flow conditions, without the presence of free surface was studied. The results obtained with the new method using different motion formulations are compared with the results obtained by the old setup ((Berchiche at al, 2017) and experimental data in Table 1.

Table 1: Comparison of integral propulsor characteristics obtained with different calculation methods. (J=0.3, straight flow, no free surface)

	KTP	KTD	KTG	KTTOT	KQP
EXP	0.317	0.183	-0.049	0.451	0.570
Old setup	0.2997	0.1761	-0.0393	0.4365	0.0567
Moving mesh/ Mesh motion	0.3039	0.1736	-0.0353	0.4421	0.0572
Overset Mesh/ Mesh motion	0.3039	0.1737	-0.0354	0.4422	0.0572
Moving mesh/ DFBI	0.3011	0.1732	-0.0358	0.4386	0.0571
Overset Mesh/ DFBI	0.3009	0.1734	-0.0356	0.4387	0.0570

The results obtained with the new setup are found to be in a slightly better agreement with experimental data than the results by the old setup. One can also conclude about a good agreement between the solutions obtained with different motion formulations. The solutions using the DFBI formulation with superposed rotation of propeller region shows a slightly lower propeller thrust (about -1.0%) than the solutions using the mesh motion model. It is also important to point out that the new setup demonstrates a faster convergence and a better stability of numerical solution, which is seen from the time histories of thrust characteristics presented in Figures 6 and 7.

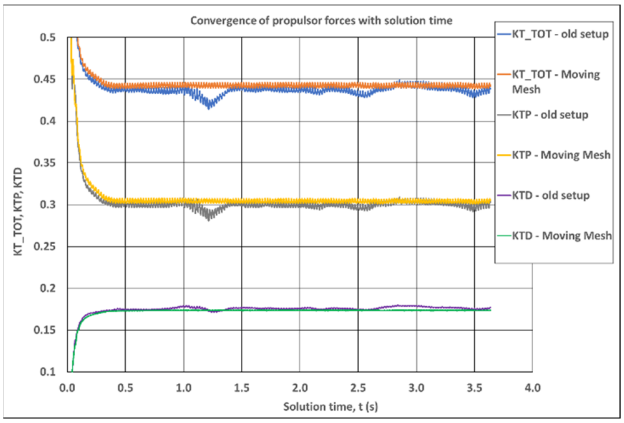

Figure 6: History of thrust convergence for propeller, duct and whole propulsor.

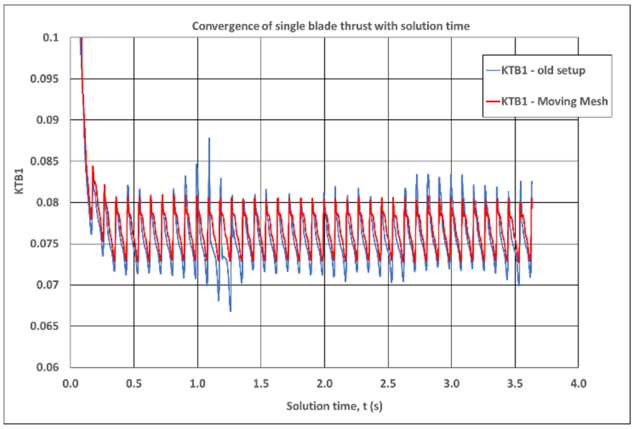

Figure 7: History of thrust convergence for single propeller blade.

The results presented above are obtained within 40 complete propeller revolutions, using the time step corresponding to 2 (deg) of propeller rotation. It has to be noted that in the problems with free surface, the time step needs to be reduced, 1 (deg) of propeller rotation being the recommended value. For further simulations of forced propulsor motions the DFBI method was chosen.

In the second test case, the propusor was subject to forced heave motion with the amplitude of 0.5Dp and frequency of 1.1Hz (1/10 of propeller rotation frequency). Such value of heave frequency is not realistic. However, it was chosen to test the numerical solutions under the condition of extreme accelerations experienced by the propulsor. The histories of total propulsor thruster and single blade thrust during two consecutive heave cycles are shown in Figure 8. It can be seen that the moving mesh method and overset mesh method bring nearly identical results. The pure heave motion causes oscillations in total thrust with the frequency about two times of heave oscillation frequency.

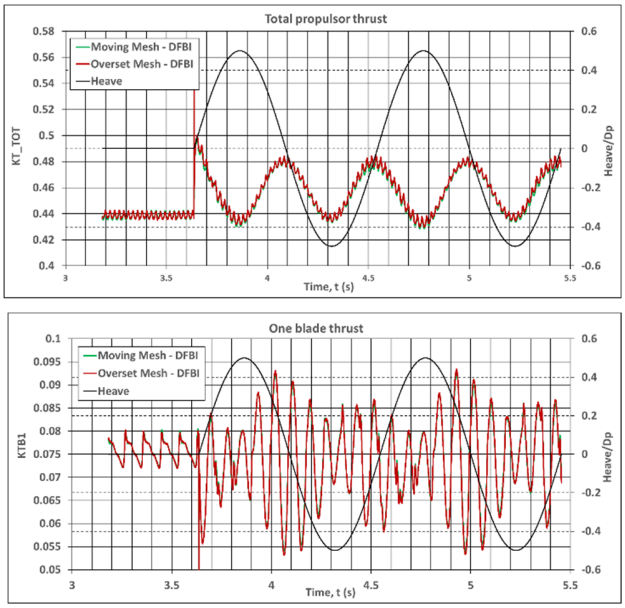

Figure 8: Histories of total propulsor thrust and single propeller blade obtained with the moving mesh method and overset mesh method. (J=0.3, Heave: Amp=0.5Dp, f=1.1Hz)

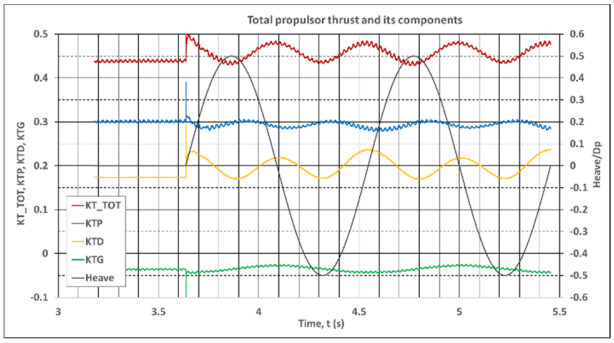

Figure 9: Histories of total propulsor thrust and its components obtained with the moving mesh method. (J=0.3, Heave: Amp=0.5Dp, f=1.1Hz)

The locations of minima of thrust values correspond approximately to the minima and maxima of heave motion. The maxima are around the zero heave where the motion velocities are highest. This pattern is largely caused by the variation of duct thrust. At those locations where the duct thrust has maximum, the propeller thrust reaches its minimum and vice versa. Higher frequency oscillations in the total thrust are due to the oscillations of blade thrust, and they are caused by the interaction between the propeller, wake of the pod housing and separated flow from the duct. The largest amplitudes of blade thrust are observed around zero heave, when propulsor is moving downwards. The smallest amplitudes are observed around the locations

of heave maxima, while somewhat larger amplitudes are seen around heave minima. Regarding the computation time, it can be remarked that the overset mesh method took about 1.5 longer time per time step than the moving mesh method. While, for complex scenarios involving ship and propulsor motions the overset mesh is definitely preferred, in the present work all simulation of forced propulsor motions were carried out with the moving mesh method.

3 PROPULSOR IN REGULAR WAVES

The geometry of the ducted pushing azimuth thruster used in the present study is detailed in (Berchiche at al, 2017). Table 2 presents the summary of calculation conditions applied in the studies on propulsor dynamics in regular waves. All CFD simulations were performed in model scale, for the propeller diameter Dp=0.25 (m) and rate of revolution n=11 (Hz).

Table 2: Calculation conditions for propulsor in regular waves.

Loading condition	Head. angle	Submer-gence, H/Dp	Wave height *), Hw (m)	Wave period *), Tw (s)	Venti-lation
Transit J=0.6	0°	1.3	1.0, 2.5, 3.0	4, 8, 10	NO
	0°	1.5, 1.3, 1.2, 1.0	1.0, 2.5, 3.0	4, 8, 10	YES
Bollard J=0.0	0°	1.2	1.0, 2.5, 3.0	4, 8, 10	NO
	0°	1.3, 1.2, 1.1, 1.0	3.0	4, 8, 10	YES

*) Wave height and period are given for full scale conditions.

We will start the discussion with considering ventilation free conditions, where the influence on propulsor is reduced to the field of orbital velocities induced by regular waves. The influence of waves of different height and period on total propulsor thrust in transit operation is illustrated in Figure 10. The thrust coefficient shown on the plot is normalized by its respective value computed in the case of free surface without waves. For the lowest wave height, there is no significant dependency of thrust on wave period, while the thrust value is reduced for about 1% compared to the case without waves. For higher waves, propulsor thrust decreases with the decrease of wave period, and in 3 (m) waves with the period of 4 (s) thrust loss of 5% is predicted. The main contribution to thrust loss comes from the reduction of duct thrust, which is caused by changes in pressure distribution over the exterior side of the duct under

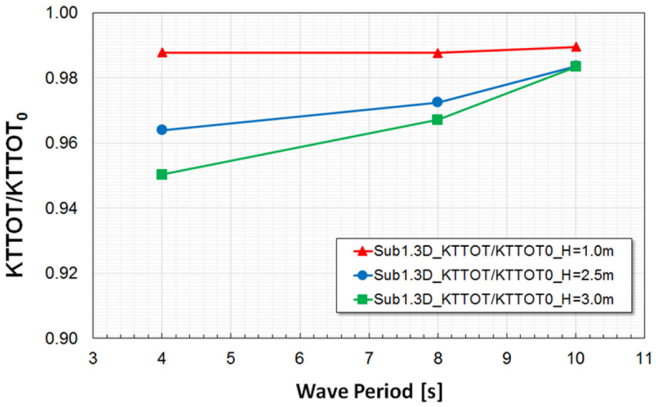

Figure 10: Influence of wave height and period on total propulsor thrust in transit operation without ventilation. (J=0.6, H/Dp=1.3)

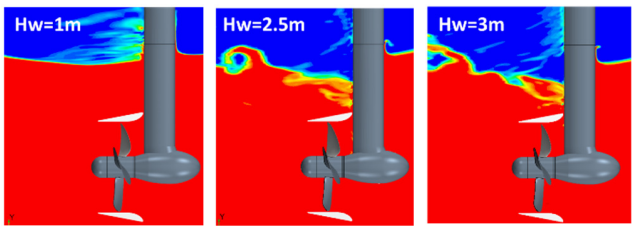

Figure 11: Deformation of free surface above propulsor in transit operation in regular waves. (J=0.6, H/Dp=1.3, Tw=4 (s))

the influence of passing waves. The images presented in Figure 11 show the deformation of free surface above the propulsor at the moment of passage of wave trough, for the case of shortest waves and different wave heights. In the case of Hw=3 (m), the propulsor already operates at the limit of ventilation inception. The air is drawn towards the propeller along the sides of the strut, and vortices develop extending from the strut to free surface, but the there is still no actual ventilation of propeller blades and duct. Figure 12 presents the variation of single blade thrust and its standard deviation depending on wave height and period. In ventilation free conditions, the averaged value of blade thrust is little affected by the wave period and wave height. For the given wave period, the amplitudes of blade thrust oscillations increase with the increase of wave height. For the given wave height, thrust amplitudes do not change significantly. When the wave period decreases, they firstly increase slightly, and then decrease again. The latter result is explained by the damping effect of limited air suction on the magnitude of wave induced orbital velocities.

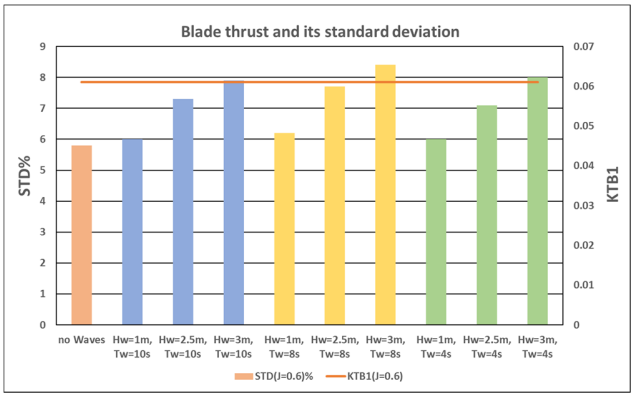

Figure 12: Influence of wave height and period on single blade thrust and its amplitude in transit operation without ventilation. (J=0.6, H/Dp=1.3; STD – standard deviation)

During bollard operation, at the submergences where ventilation does not occur, the presence of regular waves does not result in significant reduction of propulsor thrust (less than 1%), and there is no significant dependency of thrust on wave period and height, as illustrated in Figure 13 for the case of submergence of H/Dp=1.2. Unlike the observations made for transit operation, at bollard duct thrust shows only a slight reduction under the influence of waves, while propeller thrust is actually increased compared to the case without waves. This is caused by the influence of velocity field induced by the waves on the pattern of the flow around duct exterior side and duct trailing edge. It results in reduction of duct circulation, and hence in reduction of duct induced velocities on propeller. The trends in single blade thrust are similar to those described for the case of transit operation.

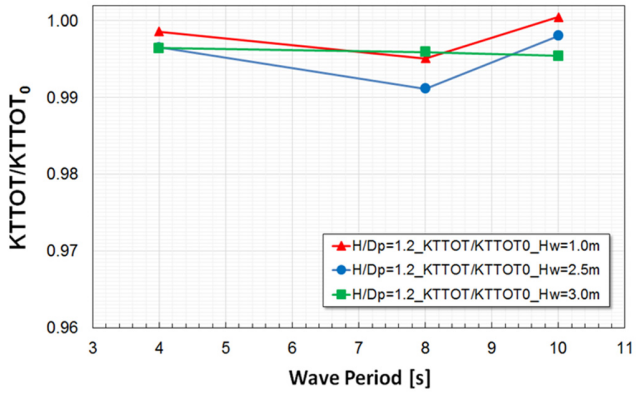

Figure 13: Influence of wave height and period on total propulsor thrust at bollard without ventilation. (J=0.0, H/Dp=1.2)

The onset of ventilation event on propulsor in regular waves depends on propulsor loading, propulsor submergence and wave parameters. For the case of waves with highest amplitude of 3(m) and shortest period of 4 (s), the diagrams showing thrust losses by propeller, duct and whole propulsor at difference submergence are presented in Figures 14 and 15.

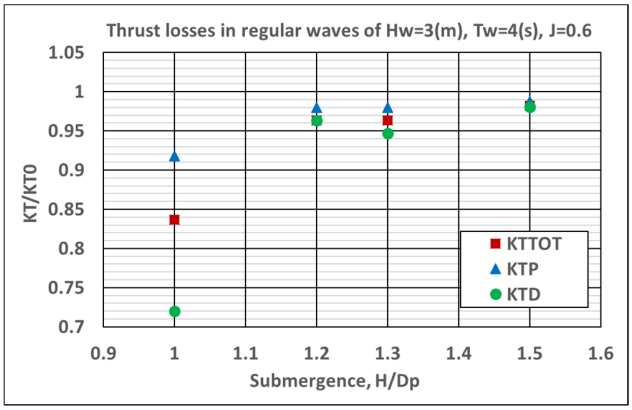

Figure 14: Thrust loss on propulsor in transit operation in regular waves with the onset of ventilation. Influence of propulsor submergence (J=0.6, Hw=3(m), Tw=4(s))

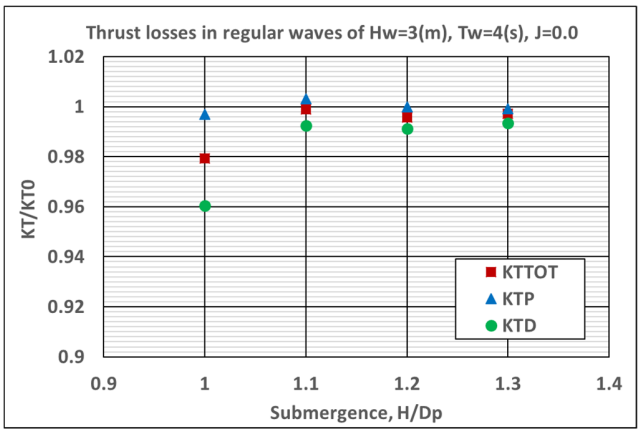

Figure 15: Thrust loss on propulsor in bollard operation in regular waves with the onset of ventilation. Influence of propulsor submergence (J=0.0, Hw=3(m), Tw=4(s))

Submergence values where a significant drop of thrust is observed correspond to stable, continuous ventilation on propulsor. At both the transit and bollard conditions, the main contribution to the total thrust loss comes from the duct. For example, at transit speed, J=0.6, and submergence of H/Dp=1.1 (with respect to the level of calm free surface), the duct loses 28% of thrust, resulting in 16% total thrust loss. Naturally, thrust loss will increase rapidly at lower submergence. At deeper submergence, intermittent ventilation may develop whose cycles occur only for a certain period of time during the passage of wave trough. A

more detailed discussion about these phenomena is presented below for the case of transit operation, J=0.6. Figure 16 present total thrust loss on propulsor as function of wave period and wave height, for the minimum studied submergence of H/Dp=1.0.

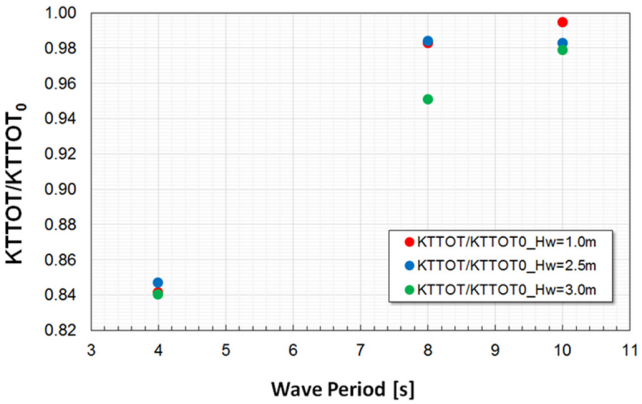

Figure 16: Thrust loss on propulsor in transit operation in regular waves with the onset of ventilation. Influence of wave parameters (J=0.6, H/Dp=1.0)

The comparable magnitudes of thrust loss observed at the wave period of 4 (s) indicate that stable, continuous ventilation develops at all wave heights. In longer waves, ventilation occurs as an intermittent event during the passage of wave troughs. Figure 17 shows the extent of ventilation on propulsor operating in 3 (m) waves with different periods. In the waves with the period of 10 (s), propeller ventilation cycle lasts for about 2 propeller revolutions, and it occurs every 18 revolutions. Thrust loss amounts 2%. In the waves with the period of 8 (s), propeller ventilation cycle last for about 8 propeller revolutions, and it occurs every 12 revolutions. Thrust loss amounts 5%. In the waves with the period of 4 (s), ventilation is continuous, without significant dependency on wave passing. Thrust loss amounts 16%. Similar to the case of calm free surface, in waves there is no considerable air entrainment by propeller along the duct inner surface.

The inception and development of ventilation on propulsor in regular waves reveals distinct differences between the conditions of transit operation and heavy loading such as bollard. If one compares the images of air fraction shown in Figure 18 for bollard condition with those shown in Figure 17 for transit condition, one can notice different trends in ventilation extent with wave period. More precisely, for a given wave height, in transit the ventilation becomes more intensive in shorter waves, while in bollard it becomes more

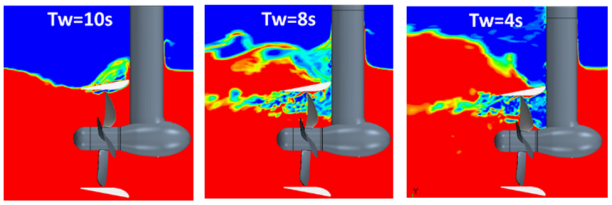

Figure 17: Ventilation extent on propulsor in transit operation in regular waves of Hw=3 (m) with different periods. (J=0.6, H/Dp=1.0)

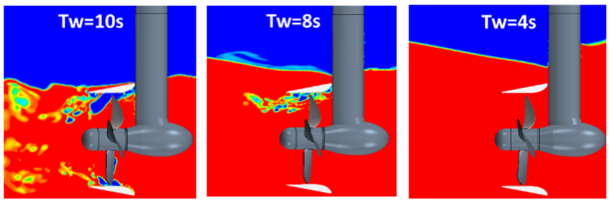

Figure 18: Ventilation extent on propulsor in bollard operation in regular waves of Hw=3 (m) height with different periods. (J=0.0, H/Dp=1.1)

intensive in longer waves. This result is explained by different ventilation inception mechanisms at heavy loading and at light loading of propulsor, and by the influence on those mechanisms of exposure time of propulsor to passing wave troughs. As shown in (Berchiche et al, 2018), in transit condition, ventilation begins as a pocket-type deformation of free surface. Shorter wave periods result in propeller being more frequently exposed to wave trough regions, so that the said pocket tends to stabilize and extend to propulsor. At bollard, ventilation begins in the form of vortices extending from the free surface to propeller, along the strut. These vortices serve as air transport ways from the free surface to propulsor. In the very beginning of ventilation event, the said vortices are very unstable. Shorter wave periods (and associated pressure variation on the strut) do not allow the vortices to stabilize and ventilation to develop. A longer exposure of the vortices to passing wave troughs in longer wave makes them more stable, so that ventilation develops and reaches the propeller easier.

The impact of ventilation on single blade thrust for propulsor in waves of different height and period is illustrated in Figure 19 for the condition of transit speed (J=0.6) and submergence of H/Dp=1.0. It can be seen that, while the averaged value of blade thrust shows only a minor reduction, the amplitudes of blade thrust oscillation increase considerably when ventilation occurs. The said increase is especially pronounced in short waves, Tw=4 (s). The values of standard deviation presented in this Figure show overall trends in blade thrust amplitude, but they may not be representative of local fluctuations.

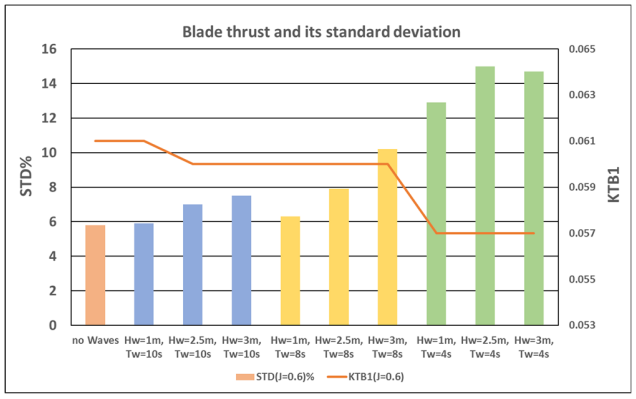

Figure 19: Influence of wave height and period on single blade thrust and its amplitude in transit operation with the occurrence of ventilation. (J=0.6, H/Dp=1.0; STD – standard deviation)

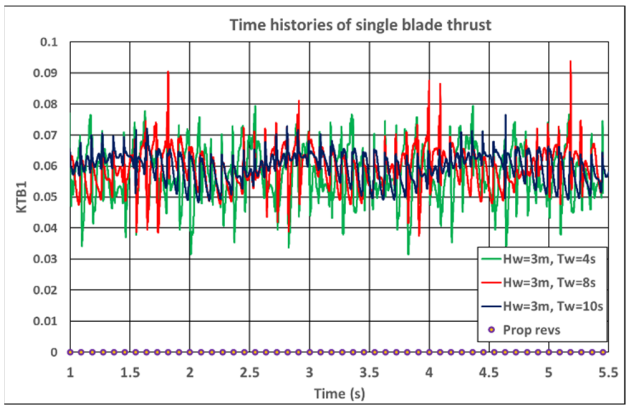

Figure 20: Time histories of single blade thrust during transit operation in 3 (m) regular waves with the occurrence of ventilation. (J=0.6, H/Dp=1.0)

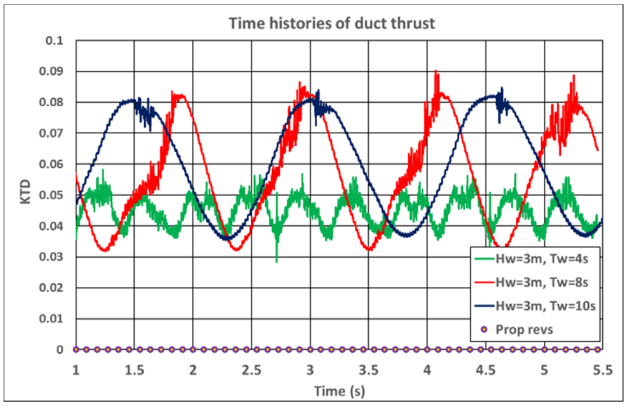

Figure 21: Time histories of duct thrust during transit operation in 3 (m) regular waves with the occurrence of ventilation. (J=0.6, H/Dp=1.0)

In order to analyze these, time histories of blade thrust and duct thrust are shown in Figures 20 and 21, respectively, for the wave height of 3 (m) and different wave periods. In longer waves, Tw=10 (s), a clear sinusoidal pattern of blade thrust history is noticed, and it matches the pattern of duct thrust, which reflects the passage of wave crests and troughs. Both the duct thrust and blade thrust increase under the influence of wave induced orbital velocities when the wave trough is approaching. After the brief ventilation event, which is marked by "spikes" in the KTD and KTB1 distributions, the thrust values begin to decrease, reaching their minima when the wave crest arrives. A sinusoidal pattern is also noticed in KTD history at wave period T=8 (s). However, the approach of wave trough is marked by the onset of ventilation on the duct, and eventually (as the trough is getting closer) on propeller. It is noticed in KTB1 history from a rapid increase of oscillation amplitudes. The largest gradients in KTB1 correspond to the instances when the blade enters the air pocket. The last phase of ventilation event, right after the trough passage, is characterized by a collapse of the air pocket inside the duct, which is noticed from sudden local peaks of KTB1. At these instances, the full amplitude of blade thrust oscillation may reach 75% of averaged thrust value. This represents a serious load which may propagate through the propeller hub and shaft to the gear system, pinion shaft and bearings. The amplitude of duct thrust oscillation, while considerably less sudden as they follow the wave frequency, amounts around 80% of averaged duct thrust value. In shorter waves, T=4 (s), ventilation is a continuous event, and sinusoidal pattern caused by wave passages is found only in the history of duct thrust. The duct thrust is reduced significantly, since the upper part of the duct is affected by the air fraction. The blade thrust reveals large oscillations (their full amplitude is about 50% of the averaged value) at blade passing frequency associated with blade going through the air pocket that stays in the upper part of propeller disk.

4 PROPULSOR SUBJECT TO FORCED PLANAR MOTIONS

The calculation matrix used in the studies with the same propulsor subject to forced planar motions is presented in Table 3. In the first part of the studies, which is discussed in this paper, the free surface was excluded from the simulation to address the pure effect of propulsor motion. The loading conditions corresponding to trawling (J=0.3) and bollard (J=0.0) operation were considered. The parameters of propulsor motions were derived from the calculation of Response Amplitude Operators (RAOs) at the location of propeller center for a typical offshore vessel (LPP=80 (m)) operating in regular waves with height

Table 3: Calculation conditions for propulsor subject to forced planar motions.

Loading condition	Head. angle	Submer-gence, H/Dp	Motion amplitudes *)	Venti-lation
Trawling J=0.3	0°	Infinite	Heave: 1.174D Sway: 0.5632D Roll: 21.198 (deg) Separate and combined	NO
Bollard J=0.0	0°	Infinite	Heave: 1.174D Sway: 0.5632D Roll: 21.198 (deg) Separate and combined	NO

of 2.5 (m) and period of 8 (s). The RAO calculations were performed using a potential vessel response code. The largest amplitudes of propulsor motions were found at the wave angle around 285 (deg), for all motion components. The vessel response calculations were performed accounting for the effect of viscous damping, but without the presence of bilge keels. This explains rather large motion amplitudes. The found amplitudes and corresponding wave frequency were used to set up propulsor motion in the CFD simulation, according to Eq. (1), using the "General Planar Motion" model of the Planar Motion Carriage method. The heave and sway motions have approximately the same phase, while roll motion has a phase shift of about -20 (deg) with respect to heave and sway, which needs to be accounted for when setting up the combined motion. Only the main results from these studies are presented in this paper.

With the given conditions, propeller performs about 29 revolutions during one complete propulsor oscillation. Three propulsor oscillations were simulated, and the results were sampled from the last two oscillations. Figure 22 shows the variation of total propulsor thrust during these two oscillations at different planar motion scenarios, for the trawling operation condition, J=0.3. The thrust experiences largest oscillations during the combined motion. The major contribution to its variation comes from the duct thrust variation due to heave motion component. In addition to large low-frequency oscillations caused by propulsor motions, the high-frequency oscillations are also found to increase compared to the case of propulsor at fixed position. These originate from the fluctuations of the blade thrust, and they are primarily caused by the interaction of the blade with the domains of separated flow behind the pod housing and inside the duct. The averaged thrust value is found to increase for about 3%, which is due to the increase of duct thrust. The propeller thrust and torque on the contrary experience reduction during the combined planar motion.

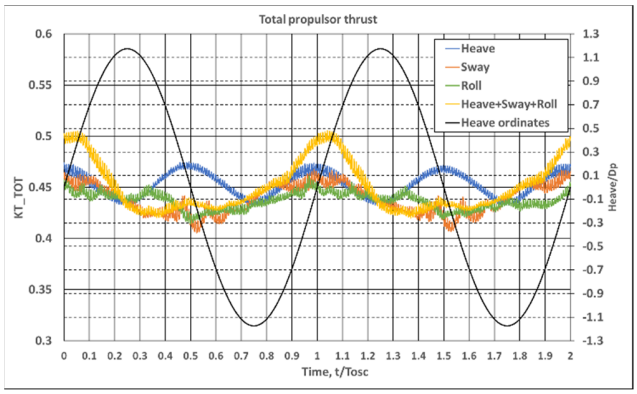

Figure 22: Time histories of total propulsor thrust during two oscillation at different planar motions. Trawling operation. (J=0.3, without free surface)

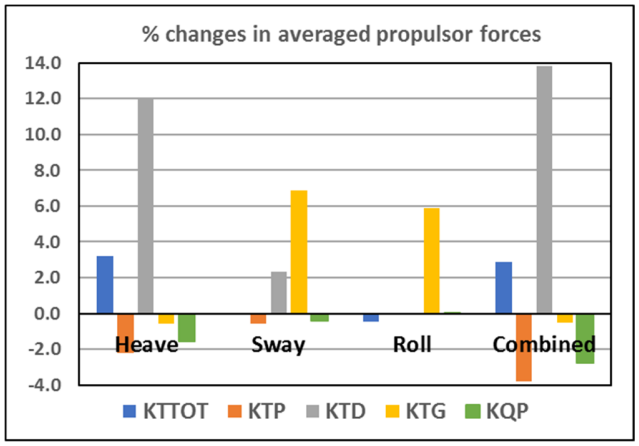

Figure 23: Relative changes in averaged propulsor loads during different planar motions. Trawling operation. (J=0.3, without free surface)

The heave motion gives the major contribution to the said changes. A more detailed information about the relative changes in average loads on propulsor components during different planar motions can be found from Figure 23. It is interesting to note that for some loads, e.g. pod resistance, KTG, and propeller thrust, KTP, the changes during the combined motion are not reduced to simple addition of changes experienced separately during heave, sway and roll. This gives an indication that hydrodynamic interaction between the motion components is important. The duct thrust, which experiences the greatest changes, reaches its maxima at the propulsor position around zero heave, where the motion velocities are highest. This increase is primarily due to additional thrust produced by the part of the duct facing in the direction of motion. The local angles of attack increase due to the cross flow caused by the vertical motion,

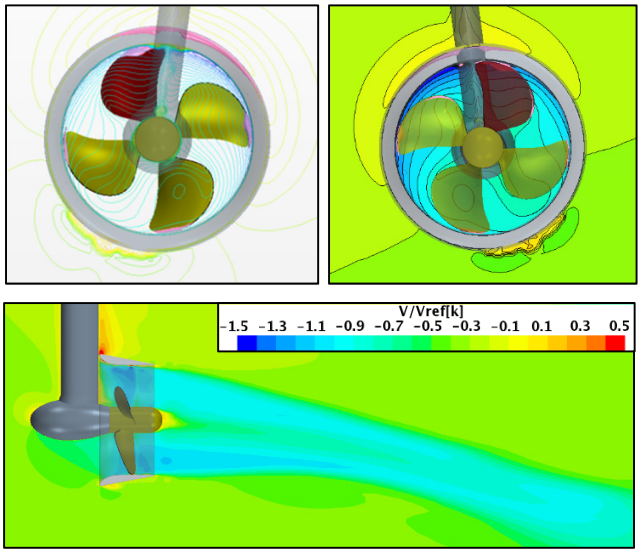

Figure 24: Images showing the velocity field and cavitation extents (Cp threshold) on propulsor during the combined (heave+sway+roll) planar motion. Trawling operation. (J=0.3, without free surface, instant corresponding to zero heave position when propulsor is moving upwards)

and pressure is reduced on the duct interior side. At the same time, separation is not developed on the interior side of the duct due to the suction effect of propeller combined with inflow velocity. The opposite part of the duct, where the local angles of attack are on the contrary reduced, experiences separation on the exterior side. However, due to the dynamic nature of this separation the loss of duct lift (and hence thrust) is smaller compare to what would take place under static conditions. Around the locations of heave minima and maxima, where the motion velocity becomes low and, eventually, changes the direction, the duct thrust approaches its value recorded for the fixed position of propulsor, but still stays slightly above it, due to the dynamic effect related to flow history. The largest extents of cavitation are predicted when propulsor passes the position of zero heave and is moving upwards, the instant shown in Figure 24. The presented cavitation extents are obtained as a volumetric threshold of pressure coefficient, since the actual cavitation phenomenon is not modelled in the numerical simulations. In this case, in addition to suction side cavitation on propeller blades that exists, while with smaller extents, near the blade tip during the whole simulation time period, pressure side cavitation on propeller blades and cavitation around duct leading edge are also predicted. The latter cavitation domains are fairly unsteady, and they disappear when propulsor moves away from the zero heave position and propulsor motion velocity becomes lower.

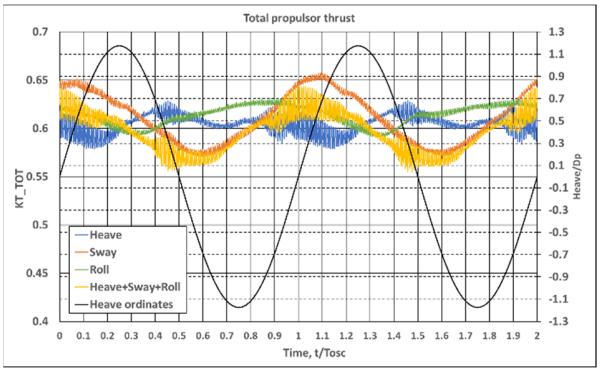

Figure 25: Time histories of total propulsor thrust during two oscillations at different planar motions. Bollard operation. (J=0.0, without free surface)

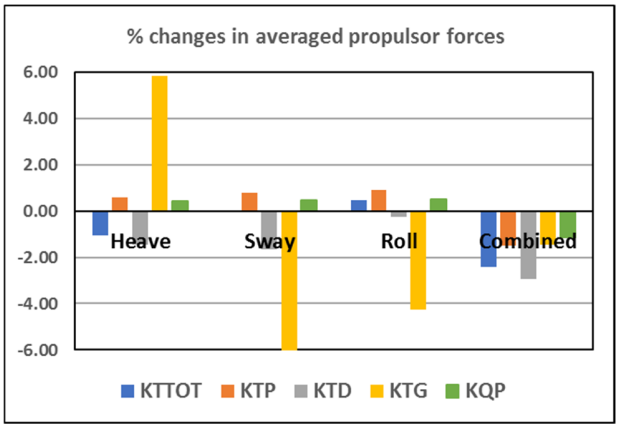

Figure 26: Relative changes in averaged propulsor loads during different planar motions. Bollard operation. (J=0.0, without free surface)

The results from similar simulations performed at bollard operation condition are presented in Figures 25 to 27. One can notice from the time histories shown in Figure 25 that, unlike the case of J=0.3, at bollard the combined motionand sway result in comparable amplitudes of total thrust oscillations. The oscillations of duct thrust and propeller thrust due to sway give the major contributions to low-frequency oscillations of total thrust during the combined motion. At the same time, compared to the case of J=0.3 one can notice larger amplitudes of high-frequency oscillations. They are associated with the oscillations of blade thrust during heave which are caused by the interaction of the blade with separated flow zone on the interior side of the duct. Flow separation inside the duct does not develop at J=0.3, but it develops at J=0.0 due to extremely large angles of attack of the duct sections during heave. The relative changes in averaged loads experienced by propulsor components at bollard (see Figure 26) are smaller than those at trawling operation.

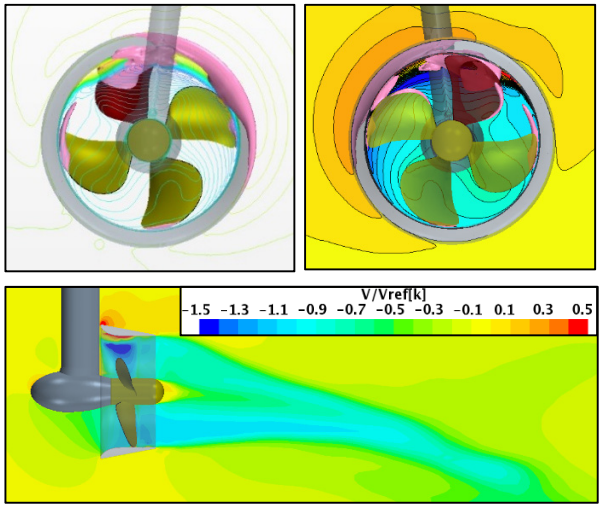

Figure 27: Images showing the velocity field and cavitation extents (Cp threshold) on propulsor during the combined (heave+sway+roll) planar motion. Bollard operation. (J=0.0, without free surface, instant corresponding to zero heave position when propulsor is moving upwards)

The duct thrust decreases during heave and sway at bollard instead of increasing as it was the case at trawling. The main reason for this decrease is that in the absence of axial inflow velocity and heavy loading of propeller, the part of the duct facing the direction of motion experiences very large angles of attack that result in flow separation on the duct interior side. This separation is the primary cause of high-frequency oscillations of blade thrust as mentioned above, but it also results in loss of lift by the duct. The separation phenomenon discussed herewith results in local increase of blade loading and considerable increase of cavitation extents on propeller blade when it passes through the separation zone. In general, cavitation on propeller and duct at bollard during the forced planar motions is more severe than it is during trawling, and the cavitation patters are more unsteady, see Figure 27. Similar to the conclusion drawn in the case of J=0.3, the trends in changes of averaged loads presented in Figure 26 indicate that hydrodynamic interaction between the component of planar motion plays an important role – compare for example the changes in propeller thrust, KTP, and torque, KQP, which increase during heave, sway and roll, but decrease in the case of combined motion.

5 CONCLUSIONS

The numerical method applied earlier to the analysis of propulsor ventilation near the calm free surface, has been generalized and extended to the cases of propulsor operation in regular waves and propulsor subject to forced planar motions. This effort results in considerable modifications in domain extension, meshing approach and solution strategies. Both the moving mesh method and overset mesh method used in the present work have shown close agreement in the test calculations. While the overset mesh method carries some computational overhead, especially when the DFBI solver is engaged, it can be recommended as a more flexible and general approach to modelling complex scenarios such as vessel with operating propulsors in waves.

During propulsor operation at transit speeds in regular waves without ventilation, the influence of wave induced orbital velocities results in the reduction of duct thrust, which increases with the increase of wave height and reduction of wave period. The fluctuations of single blade thrust show the tendency to increase with the increase of wave height at all wave period. Unlike transit operation, at bollard propulsor forces are less affected by wave induced orbital velocities.

The onset of ventilation event on propulsor in regular waves depends on propulsor loading, propulsor submergence and wave parameters. Ventilation may develop in intermittent form that lasts only during certain period during the passage of wave troughs, or in stable form that exists continuously. The onset of continuous ventilation is associated with largest thrust losses. For example, for propulsor in transit operation the loss of total thrust of 16% is predicted already at fixed submergence of one diameter, in 3 meters waves with the period of 4 (s). For the given wave height, the intensity of ventilation increases with the reduction of wave period, i.e. in shorter waves. An opposite trend is however observed during operation at bollard, where longer waves result, under otherwise identical conditions, in more intensive ventilation. This result is explained by different ventilation inception mechanisms at heavy loading and at light loading of propulsor (respectively, free surface vortices and free surface pocket), and by the influence on those mechanisms of exposure time of propulsor to passing wave troughs.

Simulations of propulsor dynamics during forced planar motions give indication that hydrodynamic interaction between the motion components (such as heave, sway and roll) plays an important role in the resulting changes in propulsor forces and their oscillations. The combined motion scenario (heave+sway+roll) reveals larger amplitudes of low-frequency oscillations associated with propulsor motion compared to individual motion components. However, major contributions to the resulting thrust dynamics are given by different motion components at low-speed operation (e.g., trawling, J=0.3) and bollard (J=0.0). It is heave at low speeds, and it is sway at bollard. The heave motion of propulsor results in increase of cavitation extents on the suction side of propeller blades, and in occurrence of cavitation on the pressure side of the blades and on the duct, where cavitation is not found when propulsor position is fixed. Planar motions at bollard reveal

more dynamic patterns of cavitation and increase of high-frequency oscillation of blade thrust caused by flow separation inside the duct. While realistic planar motions of propulsor on the ship may not be the major contributors to large thrust losses and excessive load amplitudes, they may considerably amplify the effects caused by ventilation and waves.

ACKNOWLEDGEMENT

The work presented in this paper has been conducted within the frameworks of the R&D Project "INTER-THRUST" supported by the MARTEC II ERA-NET program (Maritime Technologies). The "INTER-THRUST" Consortium includes SINTEF Ocean (Norway), Hamburg University of Technology (Germany), Voith Turbo Schneider Propulsion GmbH & Co. KG (Germany), Jastram GmbH und Co. KG (Germany), and Havyard Group AS (Norway). The support received from the Research Council of Norway for the Norwegian part of the project is greatly appreciated.

REFERENCES

ABS (2013), "Ship Energy Efficiency Measures Advisory." ABS Report.

Berchiche, N., Krasilnikov, V.I., and Koushan, K. (2017), "Analysis of Dynamic Loads on Azimuthing Ducted Propulsor under Off-Design Operation Conditions." Proceedings of the 5th International Symposium on Marine Propulsors SMP'17, Espoo, Finland, June.

Berchiche, N., Krasilnikov, V.I., and Koushan, K. (2018), "Numerical Analysis of Azimuth Propulsor Performance in Seaways: Influence of Oblique Inflow and Free Surface." Journal of Marine Science and Engineering, 2018, 6, 37; doi:10.3390/jmse6020037.

Califano, A. (2010), "Dynamic loads on Marine Propellers due to Intermittent Ventilation." PhD Thesis, NTNU, Trondheim, Norway.

Dang, J., Koning, J., Brouwer, J. and de Jong, J. (2013), "Dynamic Loads on Mechanical Azimuth Thrusters." Proceedings of the PROADS2013, CECO, Changwon City, Korea, October 20-25.

Koushan, K. (2006a), "Dynamics of Ventilated Propeller Blade Loading on Thrusters due to Forced Sinusoidal Heave Motion." Proceedings of 26th Symposium on Naval Hydrodynamics, ISBN-13: 978-0-9798095-0-7, Rome, Italy.

Koushan, K. (2006b), "Dynamics of Propeller Blade and Duct Loadings on Ventilated Ducted Thrusters Operating at Zero Speed." Proceedings of T-POD06 - 2nd International Conference on Technological Advances in Podded Propulsion, Brest, France.

Koushan, K. (2007), "Dynamics of Propeller Blade and Duct Loading on Ventilated Thrusters in Dynamic Positioning Mode." Proceedings of the Dynamic Positioning Conference, Houston, Texas, USA, October 9-10.

Koushan, K., Spence, S. and Hamstad, T. (2009), "Experimental Investigation of the Effect of Waves and Ventilation on Thruster Loadings." Proceedings of the 1st International Symposium on Marine Propulsors SMP'09, Trondheim, Norway, June.

Koushan, K., Spence, S. and Savio, L. (2011), " Ventilated Propeller Blade Loadings and Spindle Moment of a Thruster in Calm Water and Waves." Proceedings of the 2nd International Symposium on Marine Propulsors SMP'11, Hamburg, Germany, June.

van Beek, T. and van Terwisga, T. (2006), "Ventilation or Cavitation: An Experimental Study to Determine Dynamic Loads on Controllable Pitch Propellers." Proceedings of the 6th International Symposium on Cavitation, Wageningen, September.